similar relation; it does not tell us the physical mechanisms responsible for the observed shear strength. If we restrict ourselves to brittle deformation, then micromechanical mechanisms of grain rotation, grain crushing and crack growth are what result in the observed shear strength of a fault. These are the same processes that lead to brittle failure in an intact rock. The principal difference between the two cases is whether or not a fault is present and the geometrical constraints that the fault introduces. Viewed in this way, the result shown in Fig. 2 should not be surprising.

To extend this result further, consider the convergence of μ_i and μ_a in Fig. 2 at high normal stress. Byerlee[18] noted this more than 20 years ago, identifying it with the brittle–ductile transition in rock, and it has since been noted for a variety of rock types[19]. Increasing normal stress tends to suppress the dilatancy and open porosity that is required for individual grains within a gouge to roll past each other. It thus leads to more dense, interlocked grains which must deform by fracture and microcrack growth. With increasing normal stress, gouge looks and behaves more and more like intact rock, until a point is reached where it becomes as easy to break intact grains as it is to shear on existing fault surfaces. At this point (the brittle–ductile transition) we expect a convergence of μ_i and μ_a as well as a transition from localized to more distributed shear. This transition should occur whether or not crystal plasticity is taking place on the microscopic scale.

A key element of the Byerlee–Savage model is the zero-strain boundary condition

$$e_{xx} = e_{zz} = 0 \text{ (within fault gouge)} \quad (5)$$

imposed by the competent wall rock on the gouge layer. A consequence of this is that as the gouge deforms it must evolve towards a stress state in which $\sigma_{xx} = \sigma_{yy}$, a condition which can only occur when σ_1 is oriented at 45° to the fault. This boundary condition is what distinguishes the mechanics of fault deformation from deformation of material in bulk, it may imply that all mature faults develop this internal stress state, regardless of the details of the gouge constitutive law. For example, Rice[4] analysed a shear zone containing a ductile von Mises material subject to equation (5), and obtained the same stress orientation as for the Byerlee–Savage Coulomb gouge. The plastic yielding inherent in this model also tends to suppress the hydraulic fracturing that can accompany a build-up of pore pressure p within the fault zone. A necessary condition for hydraulic fracturing is $p > \sigma_3$. With increasing p, however, effective stress is reduced, causing the gouge to weaken and eventually yield. Because of the geometric constraints on the gouge[3], the plastic yielding increases σ_3 so that it remains above p.

The approach presented here represents a departure from the traditional view of friction based on ductility and plastic yielding in metals. In that view, the true area of contact between two surfaces increases with normal stress because of plastic yielding; shear strength, which is proportional to the true contact area, also increases, making the coefficient of friction relatively insensitive to normal stress. By contrast in our conceptual model the true coefficient of friction, represented by a function involving μ_i, can be relatively sensitive to normal stress. This sensitivity is then suppressed through the sin ϕ dependence imposed by the simple shear constraints of the fault zone geometry. Although plastic yielding of contact spots may be an appropriate model for friction in metals, it provides a poor representation of a fault in brittle, crustal rock. In this case, shearing on fault surfaces rapidly produces a layer of gouge which is more appropriately analysed as discussed here. This effect may explain why the steady-state velocity dependence in recent state-variable constitutive laws for friction appears to be negative for bare surfaces and yet positive for mature faults with gouge[16,20]. Stability analysis of such models[21] has shown that negative velocity dependence is necessary for fault instability. Thus it may be necessary to modify the constitutive model to include additional effects (such as fracture of asperities, fault healing and sealing, fault interactions, and fluid pressure changes) to explain earthquake instabilities. □

Received 17 December 1992; accepted 6 April 1993.

1. Hickman, S. H. *Rev. Geophys IUGG Rep.* 759–775 (1991).
2. Byerlee, J. *Geophys. Res. Lett.* **17,** 2109–2112 (1990).
3. Byerlee, J. D. *Tectonophysics* **211,** 295–303 (1992).
4. Rice, J. R. in *Fault Mechanics and Transport Properties of Rocks* (eds Evans, B. & Wong, T.-f.) 475–503 (Academic, London, 1992).
5. Byerlee, J. D. & Savage, J. C. *Geophys. Res. Lett.* **19,** 2341–2344 (1992).
6. Hansen, B. in *Pro. 5th int. Conf. Soil Mech. Found. Engng* 127–131 (Dunod, Paris, 1961).
7. Mandl, G., de Jong, L. N. J. & Maltha, A. *Rock Mechanics* **9,** 95–166 (1977).
8. Logan, J. M., Friedman, M., Higgs, N., Dengo, C. & Shimamoto, T. *U.S. geol. Surv. Open File Rep.* 79-1239, 305–343 (1979).
9. Moore, D. E., Summers, R. & Byerlee, J. D. *J. struct. Geol.* **11,** 329–342 (1989).
10. Moore, D. E. & Byerlee, J. D. *Tectonophysics* **211,** 305–316 (1992).
11. Saada, A. S., Fries, G. & Ker, C.-C. *Soils Found.* **23,** 98–112 (1983).
12. Byerlee, J. D. *Pure appl. Geophys.* **116,** 615–626 (1978).
13. Byerlee, J. D. *J. geophys. Res.* **72,** 3639–3648 (1967).
14. Summers, R. & Byerlee, J. *U.S. geol. Surv. Open File Rep.* 77-142, 129 (1977).
15. Dunn, D. E., LaFountain, L. & Jackson, R. *J. geophys. Res.* **78,** 2403–2417 (1973).
16. Marone, C., Raleigh, C. B. & Scholz, C. H. *J. geophys. Res.* **95,** 7007–7025 (1990).
17. Lockner, D. A., Moore, D. E. & Reches, Z. in *33rd U.S. Rock Mechanics Symp.* (eds Tillerson, J. R. & Wawersik, W. R.) 807–816 (Balkema, Rotterdam, 1992).
18. Byerlee, J. D. *J. geophys. Res.* **73,** 4741–4750 (1968).
19. Ismail, I. A. H. & Murrell, S. A. F. *Tectonophysics* **175,** 237–248 (1990).
20. Beeler, N. M., Weeks, J. D. & Tullis, T. E. *Eos* **73,** 511 (1992).
21. Rice, J. R. & Ruina, A. L. *J. appl. Mech.* **50,** 343–349 (1983).

Mass-spectrometric U-series dates for Israeli Neanderthal/early modern hominid sites

F. McDermott*†, R. Grün‡, C. B. Stringer§ & C. J. Hawkesworth*

* Department of Earth Sciences, The Open University, Walton Hall, Milton Keynes MK7 6AA, UK
‡ Quaternary Dating Research Centre, Australia National University, GPO Box 4, Canberra 2601, Australia
§ Department of Palaeontology, The Natural History Museum, Cromwell Road, London SW7 5BD, UK

THE nature of the relationship between Neanderthals and early modern *Homo sapiens* is controversial, yet it is fundamental to our understanding of early human evolution[1,2]. The Middle Palaeolithic sites of Israel are critical to this debate, because unlike those of western Europe and Africa they contain both Neanderthal (at Tabun[3] and Kebara[4] for example) and anatomically modern hominids (as at Skhul[5] and Qafzeh[6]). Here we present new mass spectrometric $^{230}Th/^{234}U$ dates for dental fragments from the Middle Palaeolithic burial sites of Tabun, Qafzeh and Skhul. These data, combined with published ages from electron spin resonance (ESR), provide compelling evidence that the Tabun Neanderthals and Qafzeh early modern *Homo sapiens* were approximately coeval in the southern Levant some 100 ± 5 kyr ago, but indicate that some of the Skhul material is younger. The study also shows that combined mass-spectrometric $^{230}Th/^{234}U$ and ESR dating is an invaluable technique for dating archaeological sites beyond the range of radiocarbon dating.

Uncertainties in the chronology of Tabun, Qafzeh, Skhul and other key sites have given rise to conflicting views of the Neanderthal/early modern relationship in the Levant. In the early 1980s the Tabun Neanderthals were generally considered to be 50–60 kyr old, and they were apparently succeeded by *Homo sapiens* at ~40 kyr[7] (for example, at Qafzeh and Skhul), thereby allowing the possibility that Neanderthals had contributed to the ancestry of modern humans. This view was reinforced when

† Present address: Department of Geology, University College Dublin, Belfield, Dublin 4, Ireland.

the layers containing the Kebara Neanderthal skeleton were dated at 60 ± 4 kyr by thermoluminescence[8] and at 62 ± 8 kyr by ESR[9]. But subsequent thermoluminescence dating of Qafzeh flints yielded ages of 92 ± 5 kyr[10,11] in agreement with the biostratigraphy[12]. Moreover, the Skhul and Qafzeh sites yielded ESR dates in the 80–120 kyr range[13,14], and similar or even older ages were obtained for the Tabun Neanderthal-bearing layers[15,16]. These thermoluminescence and ESR dates are still viewed with scepticism by many palaeoanthropologists[2,17,18] and a key objective of this study is to exploit the enhanced sensitivity and improved precision offered by mass-spectrometric U-series dating in order critically to evaluate the published ESR dates. U-series dates for fossil teeth reflect the time elapsed since they acquired, through groundwater, their inventory of uranium following death and burial, and so they tend to be minimum ages[19,20], although combined U-series and ESR data can overcome this problem[21]. Here, we present new high-precision (±1–2%) mass-spectrometric $^{230}Th/^{234}U$ dates for small (~50–100 mg) aliquots of mechanically separated dentine (DE) and enamel (EN) from bovid tooth samples that had been analysed previously by ESR[13–16]. In practice, more than 70% of the samples studied here yield concordant U-series and early-uptake ESR ages, which implies a closed system behaviour[21]. Furthermore, where we have obtained ages for dentine and enamel from the same tooth (samples 551 and 854; Table 1), minor discrepancies only were detected, despite large differences in U concentrations. This indicates that the U uptake history was similar for the enamel and dentine.

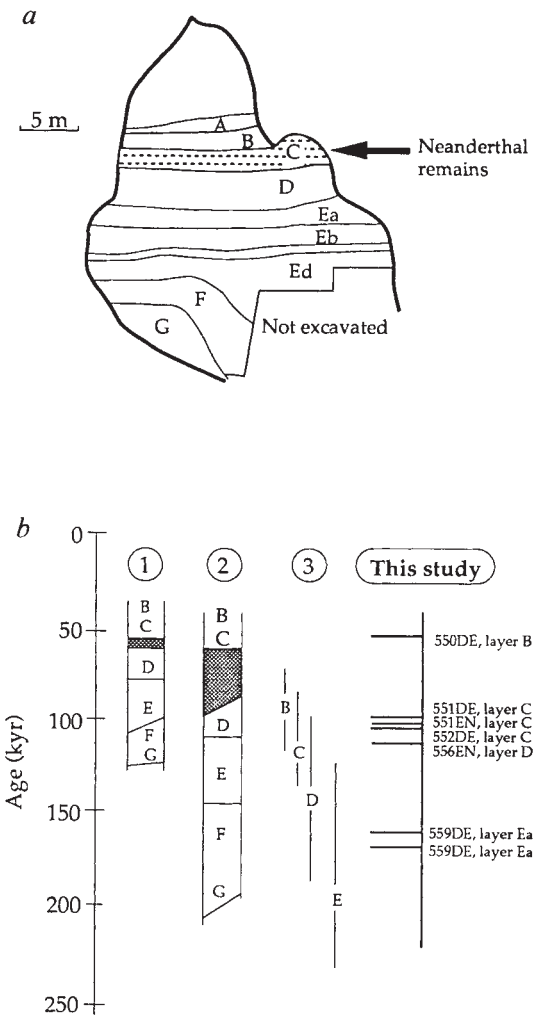

FIG. 1 *a*, Simplified stratigraphic section through the Tabun cave site after ref. 22. The Neanderthal remains are generally attributed to layer C (arrow). A more detailed stratigraphic section is provided in ref. 3. *b*, Comparison of the published chronologies of Tabun with the new U-series dates presented here. Column 1 is after Jelinek[7], column 2 summarizes Bar-Yosef's scheme[25] and column 3 represents the early uptake (EU) ESR dates in ref. 15. Shaded areas represent inferred breaks in the stratigraphy. The U-series results from this study corroborate the EU ESR ages of ref. 15 and imply that the Tabun Neanderthal.s are 100 ± 5 kyr old, or almost twice as old as previously supposed.

Detailed descriptions of the three Israeli sites studied have been given elsewhere[3,6,22–24]. The Tabun site is important because of the occurrence of well-documented Neanderthal fossils attributed to layer C (Fig. 1*a*), and because its archaeological and stratigraphic sequence has been used extensively for Late Pleistocene correlation throughout the Levant[3,25]. But the chronology of Tabun is extremely controversial (Fig. 1*b*). In Jelinek's chronology[7] (column 1, Fig. 1*b*) layers B to C date from about 40 to 60 kyr, layer D from about 65–80 kyr, and layer E from 80–100 kyr. An alternative chronology has been proposed on the basis of the archaeological sequence, microfaunal constraints and absolute dates from other sites[25] (column 2, Fig. 1*b*). In the second scheme, a relatively long hiatus is inferred between layers C and D, and so layer D is placed at about 100 kyr with layer E at 110–150 kyr. Significantly, both schemes place layer C and the associated Neanderthals in the 50–60 kyr time interval, and they contrast sharply with that based on ESR dates[15] (column 3, Fig. 1*b*). In the latter scheme layer C, and by implication the Tabun Neanderthal fossils, is ~110 kyr old, with the upper part of layer E (Ea) dated at 150–170 kyr.

In this study, two dentine samples from Tabun layer Ea yield precise U-series ages of 159.1 ± 1.3 and 168.1 ± 2.6 kyr, respectively, indistinguishable from the relatively imprecise early uptake ESR dates[15] of 158 ± 41 and 167 ± 42 kyr (Table 1). Similarly, the U-series age of 110.7 ± 0.9 kyr for sample 556EN (layer D) supports the chronology in ref. 15 (Fig. 1*b*). Moreover, three samples from the Neanderthal-bearing layer C (551DE and 551EN and 522DE) yield new U-series dates of 97.8 ± 0.4, 101.7 ± 1.4 and 105.4 ± 2.6 kyr respectively, and all are within error of the early uptake ESR ages[15] (Fig. 1*b*). Thus, the U-series dates offer compelling new evidence for the antiquity of the Tabun site, and make previously published chronologies[7,25] untenable.

Qafzeh cave (lower Galilee) has yielded the remains of at least 20 hominids[6,26] which are classified as *Homo sapiens*, albeit with some archaic cranial features[6,27]. Archaeological dating schemes had indicated an age of <50 kyr[3,7,28], although amino-acid analyses of bone[29] and microfaunal constraints suggested older ages, possibly 70–100 kyr. More recently, thermoluminescence dates on burnt flint[8] and early uptake ESR dates on mammal teeth[14] yielded average ages of 92 ± 5 kyr and 100 ± 10 ky, respectively. In this study, sample 368DE yielded a U-series age of 106.4 ± 2.4 kyr, identical to its early uptake ESR age (105 ± 2 kyr)[14]. Similarly, the U-series age for sample 371EN is 88.6 ± 3.2, within error of its average early uptake ESR age (103 ± 19 kyr)[14]. Thus, the new U-series ages for Qafzeh layer XIX are in the range 85–110 kyr, which corroborates the thermoluminescence and early uptake ESR dates, and strongly supports the contention that the Qafzeh *Homo sapiens* are significantly older than the Kebara Neanderthal, and may be coeval with those of Tabun layer C. As in the Tabun site, the new U-series dates for Qafzeh are consistent only with early uptake ESR dates and not with the linear uptake ESR dates favoured in some ESR studies[13–16] (Fig. 2).

The small cave of Es Skhul is located near Tabun[5,13]. Layer B yielded cranial and post-cranial remains of at least 10 hominids representing an archaic type of modern *Homo sapiens* and showing skeletal affinities with those from Qafzeh[6,27,30]. Two well preserved bovid teeth from layer B had been dated previously by the ESR technique and yielded early uptake ages of 88.1 ± 13.1 and 68.0 ± 5.4 for samples 521 and 522, respectively[13].

TABLE 1 New mass spectrometric U-series data for dental fragments from Tabun, Qafzeh and Skhul

Sample	^{238}U($\mu g\,g^{-1}$)	^{230}Th (pg g^{-1})	($^{230}Th/^{232}Th$)	($^{234}U/^{238}U$)	($^{230}Th/^{238}U$)	U-series age (kyr)	EU-ESR (kyr)	LU-ESR (kyr)
Tabun								
Layer B								
550DE	9.6591±13	66.568±0.170	346.75±1.87	1.0902±07	0.4085±11	$50.69\pm^{0.23}_{0.23}$	76±14	85±18
Layer C								
552DE	1.0153±05	10.906±0.150	2,475.00±35.0	1.0230±05	0.6367±88	$105.36\pm^{2.58}_{2.52}$	111±30	113±31
551EN	0.3388±01	3.692±0.016	192.15±2.66	1.0559±34	0.6459±29	$101.69\pm^{1.36}_{1.34}$	121±29	134±36
551DE	5.3366±34	58.526±0.098	96.81±0.46	1.0848±10	0.6501±11	$97.84\pm^{0.43}_{0.42}$	121±29	134±36
Layer D								
556EN	11.4621±30	137.09±0.210	4,184.00±7.00	1.0963±30	0.7089±11	$110.68\pm^{0.88}_{0.87}$	93±12	152±24
Layer Ea								
559DE{1}	7.7121±12	104.418±0.035	1,399.00±3.00	1.0372±03	0.8026±27	$159.05\pm^{1.33}_{1.31}$	158±41	158±56
559DE{2}	5.9964±09	82.546±0.034	329.67±1.54	1.0307±20	0.8160±34	$168.10\pm^{2.61}_{2.53}$	167±42	196±57
Qafzeh								
Layer XIX								
371EN	0.0675±08	0.7834±0.010	20.26±2.98	1.2098±46	0.6879±136	$88.61\pm^{3.24}_{3.12}$	103±19	125±22
368DE	1.6530±13	21.4240±0.260	42.34±0.83	1.2031±18	0.7682±93	$106.35\pm^{2.36}_{2.31}$	105±02	115±08
Skhul								
Layer B								
521DE	7.6949±12	73.360±0.280	298.826±1.14	1.0746±08	0.5651±22	$80.27\pm^{0.55}_{0.55}$	88±13	102±18
522EN	3.6995±06	21.336±0.069	369.590±1.48	1.0957±12	0.3419±11	$40.43\pm^{0.21}_{0.21}$	68±05	98±11
854DE	7.9236±13	45.360±0.031	375.940±0.11	1.0678±09	0.3393±23	$41.41\pm^{0.39}_{0.38}$	55±05	65±05
854EN	0.4815±50	2.831±0.015	64.420±0.84	1.0629±34	0.3485±19	$43.03\pm^{0.47}_{0.46}$	55±05	65±05
856DE{1}	37.9845±57	231.930±0.440	665.990±2.57	1.0932±07	0.3619±07	$43.46\pm^{0.14}_{0.14}$	46±05	66±05
856DE{2}	37.9823±45	228.090±1.460	2,993.80±15.00	1.0382±65	0.3560±23	$45.53\pm^{0.74}_{0.73}$	46±05	66±05

EN, enamel; DE, dentine. ^{238}U and ^{230}Th concentrations were determined by isotope dilution using ^{235}U and ^{229}Th tracers. $^{234}U/^{238}U$ ratios were measured in static mode with ^{234}U on the ion-counting channel of a multicollector mass-spectrometer. Chemical separation procedures for U and Th are based on those in ref. 31. Total blanks were $<2\times10^{10}$ atoms of ^{238}U and ^{232}Th, $<1\times10^{6}$ atoms of ^{230}Th and $<5\times10^{6}$ atoms of ^{234}U. Measured atomic ratios were converted to activity ratios using $\lambda_{230}=9.195\times10^{-6}\,yr^{-1}$, $\lambda_{238}=1.551\times10^{-10}\,yr^{-1}$ and $\lambda_{234}=2.835\times10^{-6}\,yr^{-1}$. Errors on the activity ratios are $\pm2\sigma$, based on the within-run counting statistics. Weighing errors, estimated at 0.15%, have been taken into account when calculating the errors on ^{238}U and ^{230}Th concentrations. Duplicate analyses (559DE and 856DE) were carried out on different portions of the dentine. Also shown for comparison are tooth enamel ESR ages[11–13].

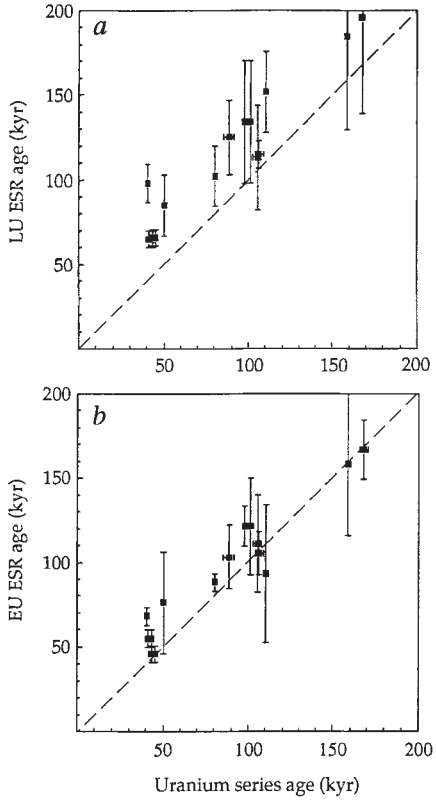

FIG. 2 *a*, Linear uptake (LU) ESR ages plotted against $^{230}Th/^{234}U$ ages for the same sample aliquots, showing that the LU ESR dates are probably too old. *b*, Early uptake (EU) ESR ages are broadly similar to the U-series ages and are within error for >70% of the samples. Error bars for the U-series ages are smaller than the data symbols except where shown.

In this study, a $^{230}Th/^{234}U$ age of 80.3±0.6 has been obtained for sample 521DE, but sample 522EN yields a relatively young age of 40.4±0.2 kyr indicative of post-depositional U uptake. Two Dicerorhinus teeth from layer B (samples 854 and 856) were also dated, and these yield rather uniform $^{230}Th/^{234}U$ dates in the range 41.4±0.4 to 45.5±0.7 kyr. Significantly, the dentine and enamel fractions of sample 854 yield similar ages (41.4±0.4 versus 43.0±0.5 kyr), despite large differences in their U concentration (Table 1). Thus, the U-series determinations combined with the published ESR data suggest a greater complexity in the stratigraphy of Skhul than was previously assumed, with clear evidence for at least two faunal ages within layer B. The younger closed system ages for samples 854 and 856 may be consistent with the suggestion that the Skhul hominids fall into earlier (Skhul 3, 6–10) and later (1, 4–5) assemblages[24], but further research will be required to investigate this possibility.

In summary, this first application of mass-spectrometric U-series dating to dental material provides strong support for the revised, more ancient chronologies for the Tabun and Qafzeh sites based on early uptake ESR age estimates. The excellent correlation between the early uptake ESR and U-series dates for more than 70% of the samples studied enhances considerably our confidence in the ages reported. Beyond the specific problems of the Middle Palaeolithic sequence of the Middle East, the feasibility of mass-spectrometric U-series dating of small dental fragments has been demonstrated, illustrating its potential for widespread further application. In detail, the data indicate that the mode of U uptake by dental materials is site-specific, and that the use of generalized U uptake models is hazardous. Finally, the conclusion that early modern *Homo sapiens* were probably coeval with and locally pre-dated Neanderthals in the Levant now seems inescapable, which in turn requires that the simple ancestor/descendant evolution models be abandoned. □

Received 25 January; accepted 10 March 1993.

1. Stringer, C. B. & Grün, R. *Nature* **351,** 701–702 (1991).
2. Wolpoff, M. H., Frayer, D. W. & Stringer, C. B. *Nature* **356,** 200–201 (1992).
3. Jelinek, A. J. *Science* **216,** 1369–1375 (1982).

4. Rak, Y. *Am. J. phys. Anthrop.* **81,** 323–332 (1990).
5. McCown, T. D. & Keith, A. *The Stone Age of Mount Carmel* Vol. II (Clarendon, Oxford, 1939).
6. Vandermeersch, B. *Les Hommes Fossiles de Qafzeh, Israel* (CNRS, Paris, 1981).
7. Jelinek, A. J. in *The Transition from Lower to Middle Palaeolithic and the Origin of Modern Man* (ed. Ronen, A.) 57–101 (Brit. Archaeol. Rep. Int. Ser. 151, Oxford, 1982).
8. Valladas, H. *et al. Nature* **330,** 159–160 (1987).
9. Schwarcz, H. P. *et al. J. archaeol. Sci.* **16,** 653–659 (1989).
10. Valladas, H. *et al. Nature* **331,** 614–616 (1988).
11. Aitken, M. J. & Valladas, H. *Phil. Trans. R. Soc. Lond.* B**337,** 139–144 (1992).
12. Bar-Yosef, O. & Vandermeersch, B. in *Prehistoire du Levant* (eds Cauvin J. & Sanlaville, P.) 281–285 (CNRS, Paris 1981).
13. Stringer, C. B. *et al. Nature* **338,** 756–758 (1989).
14. Schwarcz, H. P. *et al. J. hum. Evol.* **17,** 733–737 (1988).
15. Grün, R, Stringer, C. B. & Schwarcz, H. P. *J. hum. Evol.* **20,** 231–248 (1991).
16. Grün, R. & Stringer, C. B. *Archaeometry* **33,** 2, 153–199 (1991).
17. Jelinek, A. J. in *The Emergence of Modern Humans* (ed. Mellors, P.) 81–90 (Edinburgh Univ. Press, Edinburgh, 1990).
18. Jelinek, A. J. in *The Evolution and Dispersal of Modern Humans in Asia* (ed. Akazawa, T.) (Univ. Mus. Bull. Univ. of Tokyo, in the press).
19. Rae, A. M. & Ivanovich, M. *Appl. Geochem.* **1,** 419–426 (1986).
20. McKinney, C. R. thesis, SMU Dallas (1991).
21. Grün, R. *et al. Nucl. Tracks* **14,** 237–241 (1988).
22. Garrod, D. & Bate, D. *The Stone Age of Mount Carmel* Vol. I (Oxford Univ. Press, Oxford, 1937).
23. Farrand, W. R. *J. archaeol. Sci.* **6,** 369–392 (1979).
24. McCown, T. D. in *The Stone Age of Mount Carmel* Vol. I (eds Garrod, D. & Bate, D.) 91–107 (Clarendon, Oxford, 1937).
25. Bar-Yosef, O. in *The Human Revolution: Behavioral and Biological Perspectives on the Origin of Modern Humans* (eds Mellar, P. & Stringer, C. B.) 589–610 (Edinburgh Univ. Press, 1989).
26. Oakley, K. P. *et al. Catalogue of Fossil Hominids III: Americas, Asia and Australia* (British Museum (Nat. History), London, 1975).
27. Stringer, C. B. & Trinkaus, E. in *Aspects of Human Evolution* (ed. Stringer, C. B.) 129–165 (Taylor and Francis, London, 1981).
28. Jelinek, A. J. in *Prehistoire du Levant* (eds Cauvin, J. & Sanlaville, P.) 265–280 (CNRS, Paris, 1981).
29. Masters, P. M. in *The Transition from Lower to Middle Palaeolithic and the Origin of Modern Man* (ed. Ronen, A.) 43–54 (Brit. Archaeol. Rep. Int. Ser. 151, Oxford, 1982).
30. Trinkaus, E. in *The Origin of Modern Humans* (eds Smith, F. H. & Spencer, F.) 251–293 (Liss, New York, 1984).
31. Edwards, R. L. *et al. Earth Planet. Sci. Lett.* **81,** 175–192 (1987)

ACKNOWLEDGEMENTS. We thank T. Bradshaw, M. Johnston, P. van Calsteren and D. Wright for assistance in the radiogenic isotope laboratory at the Open University.

Positive genetic correlation between female preference and preferred male ornament in sticklebacks

Theo C. M. Bakker

University of Bern, Zoologisches Institut, Abteilung Verhaltensökologie, Wohlenstrasse 50a, CH-3032 Hinterkappelen, Switzerland

A NUMBER of population genetics models predict the evolution of male sexual ornaments through female choice[1], but their genetic assumptions and predictions have hardly been investigated[2,3]. A key feature of these models is a positive genetic correlation between male ornaments and female preference for them[4]. Here I test this prediction at the within-population level with three-spined sticklebacks, *Gasterosteus aculeatus*, which show conspicuous sexual dichromatism[5]. Intense red males are preferred in various situations[6–10], but there is great intrapopulational variation in redness both among wild-caught[6,10] and among laboratory-bred males[11], which is partly environmental[6] and may be partly genetic[12,13]. Also, females show considerable intrapopulational variation in their preference for redder males[6,8,9], which is partly environmental[8,9]. Wild-caught, intense red males and dull males were crossed with a number of females from the same population in a full-sib/half-sib breeding design. Daughters were tested for their preference for more intensely red males, and the sons' coloration was quantified. Both traits showed genetic variation. Also the redness of the sons correlated with the preference for red of their sisters, thus the two traits show positive genetic correlation.

Sexually mature sticklebacks were caught in the spring of 1990 from a Swiss freshwater population (near Roche/Montreux, 46°26′ N, 6°55′ E) which was introduced more than a century ago[14]. In the laboratory, fish were kept under simulated summer conditions; males were housed singly in small tanks, whereas females were stored in female groups[6]. After nest building, males were used in sequential mate choice tests of ripe females[8].

Six of the most extremely coloured males, that is, three intense red and three pale red males, served as fathers. They were crossed in a full-sib/half-sib breeding design[15] with 14 females, which covered the whole spectrum of preference phenotypes for redder males as determined in sequential choice tests[8]. Paternal effects on offspring traits were excluded by removing clutches from the fathers' nests after fertilization. Progenies were raised and maintained in several small standardized full-sib groups per cross. Before the attainment of sexual maturity the sexes were separated; of each cross a random sample of males was housed individually and a random sample of females was maintained in standardized sister groups.

Two weeks after the completion of the first nest, the males' maximal intensity of red coloration on the throat was quantified[16]. Redder fathers produced on average significantly redder sons (Fig. 1), thus indicating additive genetic variation for red intensity. An analysis of variance (ANOVA) of red intensity of sons in full-sib and half-sib families also revealed a significant added variance component among fathers, indicating additive

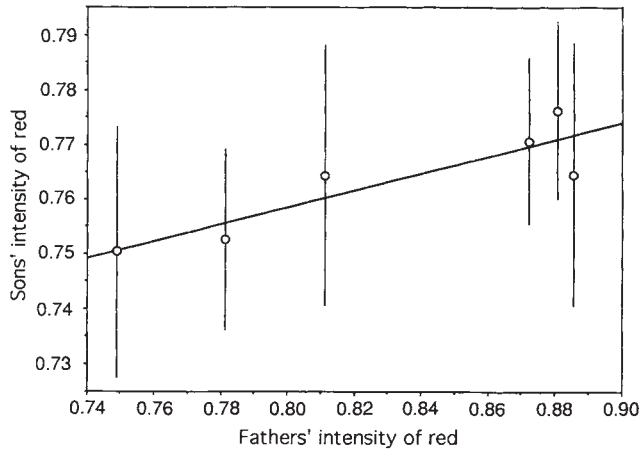

FIG. 1 Correlation between the intensity of red breeding coloration of wild-caught fathers and their laboratory-bred sons (average score of sons per father ±s.d.) ($r^2=0.79$, $F=15.02$, d.f.=1, 4, $P=0.009$, 1-tailed). Number of tested sons (number of crosses) from left to right: 21(3), 7(1), 20(3), 9(2), 8(1), 38(5). Paternal effects were ruled out by removing clutches from the nests 1 h after fertilization, and hatching them artificially[11]. The fish were raised in small standardized full-sib groups under simulated summer conditions (16:8 h in light/dark cycle, 15 °C) and fed freely. Because parasites might affect male coloration[6], only food items were used that were most likely to be free of parasites. The few fish that caught or were suspected to have caught an *Oodinium* infection were not used in the tests. At first signs of developing breeding coloration, about 7 months after hatching, the sexes were separated, and a random selection of males individually housed[6]. Each row of 6 male tanks was illuminated by a 40 W fluorescent tube mounted 10 cm above the tanks. The males were regularly stimulated with ripe females, and most of them had built a nest within 2 months of isolation. Fathers' and sons' intensity of red was quantified 2 weeks after the completion of the first nest using Frischknecht's procedure[16]. Slides of the males were taken in a standardized set-up and analysed with a densitometer[16]. In the red throat region, the optical density of red (R, filter 700 nm), green (G, filter 546.1 nm), and blue (B, filter 435.8 nm) was measured at 10 defined points (diameter 0.5 mm). An appropriate measure of the intensity of red that is independent of the brightness of a colour, is the red index[16], in which the R value (corrected for differences in film development) is expressed relative to the total colour density (R+G+B) and substracted from 1 to obtain positive values between 0 and 1. The highest index for red on the throat was used in the analyses. A proof of the reliability of the method was obtained by a direct comparison[10] of the red index with chroma calculated from reflectance spectra[34,35] (Spearman rank correlation coefficient $r_s=0.80$, $N=15$, $P<0.0015$, 1-tailed).